λ_c (μm)	Plate spacing (in λ_c's)	$V_{mla,max}/V_{mta,max}$	$V_{mla,max}/V_{mcb,max}$
112	2 (Designs 2,3)	48	3.2
112	1 (Design 1)	35	2.4
922	1/4 (Designs 2,3)	102	6.8
922	1/8 (Design 1)	54	3.6

Table 5.1: Depolarization ratios for plate spacings corresponding to the electrode designs in chapter 4 and for two different values of the length constant. $V_{mla,max}$ is the maximum depolarization induced in an axon model by a longitudinal field, $V_{mta,max}$ is the maximum depolarization induced by a transverse field, and $V_{mcb,max}$ is the maximum depolarization induced in a cell body model.

in size. As we will see below, small electrodes were desired when positioning the stimulating electrodes. The electrode dimensions listed in Table 4.1 represent a design tradeoff between the constraints of large wire spacing and small electrode tip size.

Table 5.1 summarizes the depolarization ratios which result from several nonideal plate spacings. The first and second rows of the Table present the ratios for plate spacings corresponding to the wire spacings of the chapter 4 electrodes. The length constant used to calculate these ratios was 112μm as before. After the electrodes were constructed, it was discovered that the membrane conductance per unit area for ganglion cell axons may be closer to $1/(68,000\Omega\cdot\text{cm}^2)$ [9], much lower than the value listed in Table 3.2. In this case, the length constant would be 922μm. The resulting depolarization ratios for the chapter 4 electrodes are listed in the third and fourth rows of Table 5.1. Note that, even though the plate spacings are reduced to 1/4 (designs 2 and 3) and 1/8 (design 1) of the length constant, the depolarization ratios are larger than those listed in the first two rows. While increasing the length constant causes a decrease in the effective plate spacing, which would lower $V_{mla,max}$ for a fixed λ_c, we also see from equation (3.29) that $V_{mla,max}$ increases in proportion to λ_c for a fixed d.

Table 5.1 suggests that for all length constants and electrode wire spacings considered, the same qualitative differences in thresholds will be found. The analysis portion of this thesis therefore leads to three hypotheses which can be tested in experiments using the electrodes of chapter 4:

Hypothesis 1 *The threshold for stimulating cell bodies is lower than that for stimulating axons when the electrode wires are parallel to the axons.*

Hypothesis 2 *The threshold for stimulating axons is higher when the electrode wires are parallel to the axons than when when the wires are perpendicular to them.*

Hypothesis 3 *The threshold for stimulating cell bodies is higher than that for stimulating axons when the electrode wires are perpendicular to the axons.*

Note that, unlike in chapter 3 or in Table 5.1, we are not predicting the relative thresholds in quantitative terms. Due to both the large number of assumptions which were made to facilitate analysis (see sections 3.1 and 3.5) and also to the fact that the parallel wires are only an approximation to the parallel plates, we expect that experiments would at best yield qualitative verification of the hypotheses.

5.2 Outline of the experimental procedure

All experiments followed the same basic procedure. This procedure is outlined below:

1. **Dissection.**

   Experiments were done *in vitro*. Retinas were removed from either rabbits, as described in [27], or turtles, as described in [4], and mounted on a holder over which physiological fluids were perfused. Such fluids help to prolong the life of the retina after removal from the eye.

2. **Position the recording and stimulating electrodes.**

   Testing the hypotheses of the previous section requires the use of two types of electrodes. A stimulating electrode, such as those described in chapter 4, is used to deliver current to a ganglion cell, while a recording electrode is used to determine if the cell produced an action potential as a result. In all experiments, the recording electrode was placed outside of but very close to a ganglion cell body or axon. Furthermore, the recording and stimulating electrodes were always placed as far apart from one another as possible to circumvent the problem of stimulus artifact, which will be discussed in section 5.3.

   Experimental efforts concentrated mainly on Hypothesis 2 above. To test this hypothesis, the recording electrode was positioned near a cell body, and stimuli were delivered to the axon at a distant location. Action potentials generated by the stimulating electrode and picked up by the recording electrode in this arrangement were conducted *antidromically*, or towards the cell body. The stimulating electrode was oriented so that the wires were either parallel to the axon, as in Figure 5-1a, or perpendicular to the axon, as in Figure 5-1b.

   In order to test Hypotheses 1 or 3, it would be necessary to record action potentials from the axon at a location near the optic disk. In this case the stimulating electrode would be placed closer to the cell body. Action potentials generated by the stimulating electrode and picked up by the recording electrode in this arrangement would be conducted *orthodromically*, or away from the cell body. The stimulating electrode would either be placed over the cell body, as in Figure 5-1c, or over a segment of the axon, as in Figure 5-1d. Note that the stimulating electrode in Figure 5-1d is oriented so that the wires are parallel to the axon. This orientation would be used to test Hypothesis 1. To test Hypothesis 3, the electrode wires would be oriented perpendicular to the axon (not shown).

3. **Determine threshold.**

   The amplitude of the stimulus was then adjusted until the minimum amount of current required to produce action potentials was found.

4. **Move the stimulating electrode.**

   The stimulating electrode was then shifted from one of the positions and orientations described above to another, and threshold determination repeated.

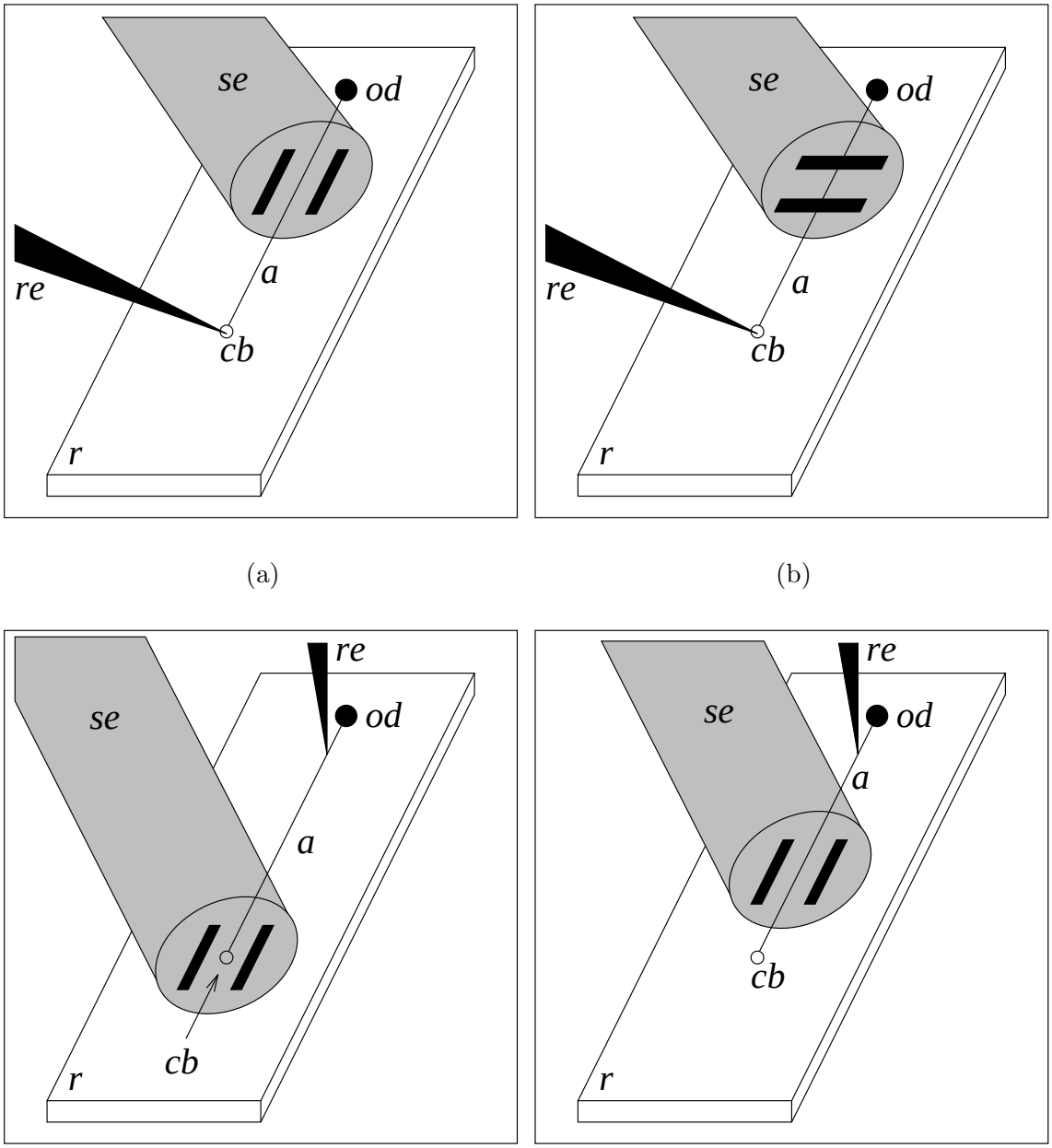

Figure 5-1: Schematic diagrams illustrating several arrangements of the recording and stimulating electrodes. Abbreviations: *cb* - cell body; *a* - axon; *od* - optic disk; *re* - recording electrode; *se* - stimulating electrode; *r* - retina.

5.3 Unresolved experimental issues

Several difficulties were encountered during experimentation which hindered our ability to obtain conclusive results. Many of these point to problems with our current experimental methods which have yet to be resolved. A discussion of these unresolved experimental issues is undertaken in this section.

5.3.1 Stimulus artifact

When current is applied to the stimulating electrode in preparations such as those of Figure 5-1, electrical activity is invariably picked up by the recording electrode. This activity is called the *stimulus artifact*. The stimulus artifact may outlast the stimulating current itself and can be substantially larger than extracellularly recorded action potentials. The former effect is thought to be due to saturation of recording amplifiers [46]. Because action potentials propagate along an axon with a finite velocity, it will take a finite amount of time for them to travel from their site of origin, near the stimulating electrode, to the recording electrode. If the two electrodes are placed far enough apart, the artifact will have died out by the time action potentials are recorded. This was the case for the experiments on rabbit retina, where the distance separating the electrodes was about 1cm. If the stimulating and recording electrodes are fairly close to one another, on the other hand, action potentials will arrive at the recording electrode while the stimulus artifact is still dominant. This was the case for the turtle retina experiments, where electrode separation was less than 0.5mm. Unfortunately, the stimulating and recording electrodes could not be placed further apart due to the small size of the turtle retina preparation. In this second case, we could not tell whether or not we were generating action potentials because, if they were occurring, they were obscured by the stimulus artifact.

5.3.2 Position of the stimulating electrode relative to the cell

The locations of ganglion cells were not known *a priori*. Had we been able to visually identify cells under a microscope, the recording and stimulating electrodes could have been positioned as discussed in section 5.2 in a straightforward manner. With the exception of the rabbit retinal ganglion cell axons, however, the cells of the rabbit and turtle retinas are completely transparent. The rabbit axons are ensheathed in white myelin near the optic disk, but are also grouped in clusters which makes them hard to identify individually. On the other hand, various staining techniques have been used for visualizing cell bodies. For example, see [28]. It was found that the staining process altered the sensitivity of cells to electrical stimuli [26]. For this reason, we did not stain ganglion cells in our experiments.

Because the locations of individual cells were unknown, a certain amount of guesswork was required when positioning the recording and stimulating electrodes. The recording electrode, for example, was positioned by repeatedly lowering it onto different portions of the retina until it was close enough to a cell body or axon to record action potentials from it reliably. This method, though at times tedious, was fairly consistent. More problematic was the positioning of the stimulating electrode.

Position in the plane of the retina

The placement of the stimulating electrode in the plane of the retina depended in part on the position of the recording electrode. For example, if recordings were being made from a

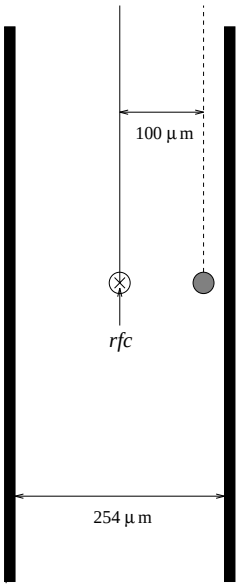

Figure 5-2: Two possible positions of the cell body (white and shaded circles). A stimulating electrode with wire spacing 254μm centered over the receptive field center (*rfc*).

cell body, as in Figures 5-1c and 5-1d, the path of the axon was approximated as the straight line from the recording electrode to the optic disk. On the other hand, if recordings were being made from an axon, as in Figures 5-1a and 5-1b, the cell body location was inferred from the location of the cell's receptive field center, and the axon was assumed to follow the straight line between the cell body and recording electrode. The stimulating electrode was placed over the desired region of retina based on these approximations.

An example will help to illustrate the potential difficulties involved in the placement methods described above. Consider an experiment in which we wish to stimulate a ganglion cell near the cell body, as in Figure 5-1c. The exact location of the cell body is unknown, but the center of the cell's receptive field can be determined by shining a small spot of light on different parts of the retina while monitoring cellular responses with the recording electrode. For rabbit retina, we estimate that ganglion cell bodies are within about 100μm (in the plane of the retina) of the cell's receptive field center [26]. Suppose that, in the absence of more detailed knowledge of the cell body location, a stimulating electrode with wire spacing 254μm (design 2 or design 3) is centered over the receptive field center. Figure 5-2 illustrates both the ideal situation, in which the cell body (white circle) is at the same location as the receptive field center, and a less desirable situation, in which the cell body (shaded circle) is displaced 100μm from the receptive field center.

The stimulating fields experienced by the cell in the two cases may be quite different, leading to ambiguities in the interpretation of thresholds. If the cell is centered between the wires, for instance, we might expect the uniform field approximation to be a good one. On the other hand, if the cell is closer to one of the electrode wires, we might expect fringing fields to be substantial (see Figure 4-2 for hypothesized stimulating fields). Since the position of the stimulating electrode relative to the cell will determine the shape of the effective stimulating field, we might expect thresholds to vary with electrode position.

However, since for a given experiment the electrode position relative to the cell is unknown, we would be unable to determine which thresholds corresponded to which positions.

Ambiguities of this sort might be eliminated if the stimulating electrode wires were spaced far enough apart. However, increasing the wire spacing will increase the overall size of the electrode tip. To some extent, our ability to place the electrode over the receptive field center accurately depends on the size of the electrode tip. The larger the tip, the less accurate electrode placement will be.

Another way to tackle this problem might be to record the thresholds at a series of points on the retinal surface, and then try to deduce the location of a cell body or axon by hypothesizing how the thresholds will change with position. This strategy involves moving the stimulating electrode from its initial position, which entails additional complications. These are considered in section 5.3.3.

Placement above the retina

The discussion thus far has focused on the position of the electrode relative to the cell in the plane of the retina. The height of the electrode above the cell is also an important consideration in the interpretation of threshold measurements. In general, we expect the threshold to rise as the electrode height is increased, since an increase in the electrode-to-cell distance is accompanied by a decrease in the effective stimulating field. In order to impose some measure of consistency on the electrode-to-cell height, attempts were made to place the stimulating electrode directly against the inner limiting membrane. Using such a scheme, the variability in the vertical electrode to cell height is constrained to the variation of cell body or axon depths within their respective layers (see Figure 2-3).

Two different methods were used to place the electrode against the inner limiting membrane. In both cases, the task amounted to lowering the electrode as close to the retina as possible without compressing so much that cell damage resulted. The first method, used with the turtle preparation, involved lowering the electrode under visual control. As the electrode was lowered, we watched for visible signs that the edges of the electrode tip were compressing the retina. It was important for the electrode tip to have small diameter for this method, so that the entire tip could be seen at a reasonably high magnification. In general, this method was complicated by the fact that the retina itself is transparent, and also by the fact that the optics were often blurred by the electrode tip or by the fluids flowing over the retina. It remains unclear whether or not the electrode tip was indeed against the inner limiting membrane when this method was used. The second method, used with the rabbit retina, relied on threshold information to infer electrode height. Thresholds were measured as the electrode was moved progressively closer to the retina. Up until a certain point, thresholds decreased as the electrode was lowered. When the threshold stopped decreasing, the electrode was assumed to be apposed to or slightly compressing the inner limiting membrane.

Control experiment

A control experiment was performed to determine the precision of the second method. Using that method, the electrode was repeatedly lowered onto and withdrawn from the same spot on the retinal surface using a micromanipulator. The micromanipulator could be used to maneuver the electrode in any of three orthogonal directions, the manipulator *axes*. Motion along each axis was controlled with a separate knob, and the distance moved in each

Trial	Threshold (μA)	z-micrometer (mm)
1	140	6.740
2	160	6.694
3	165	6.712
4	165	6.743

Table 5.2: Results from a control experiment conducted to determine how precisely the electrode could be placed against the inner limiting membrane using the second method described in the text. Lifting the electrode off of the retina corresponded to lowering the micrometer reading. Trials are listed in chronological order.

direction could be measured from a micrometer. A single direction, which we referred to as z and which was approximately perpendicular to the table, was used in this experiment. Each time the final height was determined, with the electrode presumably against the inner limiting membrane, the threshold and z-micrometer reading were recorded. Table 5.2 summarizes these results.

Several observations may be made from the Table. Most importantly, the final z-micrometer readings for the 4 trials varied over a range of about 50μm. Assuming that the inner limiting membrane had not moved relative to the table on which the micromanipulator rested, this value would ideally have been constant. Is 50μm a tolerable amount of uncertainty? In other work, such a difference in electrode height led on the average to a 2.5-fold increase in threshold [64]. We see from Table 5.2 that the total change in threshold over the 4 trials amounted to a less dramatic increase. However, note that in this experiment the threshold did not necessarily increase with the electrode height. From Trial 2 to Trial 3, the electrode was lowered 18μm closer to the retina while the threshold increased by 5μA. Rather than increasing with electrode height, the thresholds appear to be increasing with time. We will return to this subject in section 5.3.4.

On the whole, the control experiment was inconclusive. Thus the precision of the second method described above for placing the stimulating electrode against the inner limiting membrane still remains in doubt.

5.3.3 Movement of the stimulating electrode

It was often necessary to move the stimulating electrode from its initial position and orientation to another one. This might have been done to determine the location of a cell as described above, or simply in order to shift the stimulating electrode between the arrangements of Figure 5-1. In order to avoid dragging the retina, the electrode was lifted off of the tissue before making such changes, and then then lowered again.

In order to properly interpret changes in threshold with electrode position or orientation, we must have a detailed knowledge of how the electrode moved relative to the cell. To illustrate this point, consider an experiment to test Hypothesis 2. Cross sectional views of the stimulating electrode in the configurations of Figures 5-1a and 5-1b are shown in Figures 5-3a and 5-3b, respectively. Suppose that, as drawn in Figure 5-3, the height of the electrode has been inadvertently raised after rotation of the wires. If the threshold rose from Figure 5-3a to Figure 5-3b, we would not be able to conclude whether the increase was

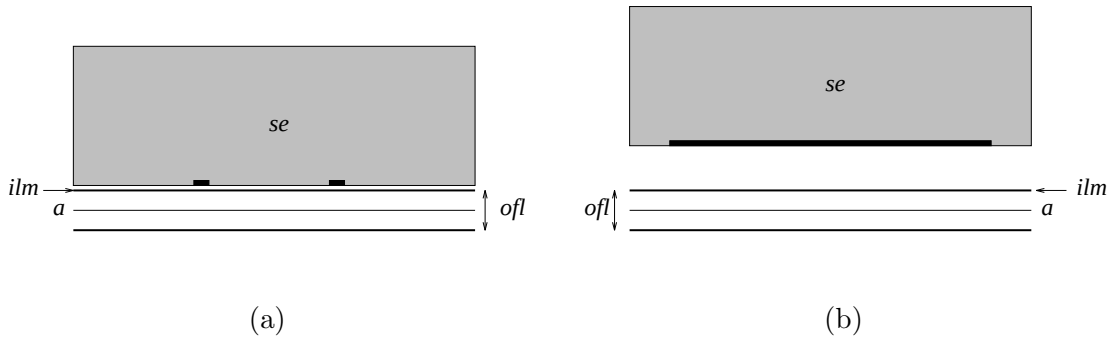

(a) (b)

Figure 5-3: Examples of electrode placement over the retina. (a) Electrode oriented so that its wires are perpendicular to an axon, as in Figure 5-1a; (b) electrode oriented so that its wires are parallel to the axon, as in Figure 5-1b. Abbreviations: *a* - axon; *se* - stimulating electrode; *ilm* - inner limiting membrane; *ofl* - optic nerve fiber layer.

due to the change in electrode orientation or to the increase in electrode height. Results would be inconclusive in this case.

A further objection to moving the stimulating electrode is that, as mentioned above, it must be lifted off of and then lowered back down onto the retina. If it were lifting or compressing the retina in the process, this might result in cell damage. Again ambiguities would arise in the interpretation of threshold measurements. Thresholds might increase due either a change in electrode position or due to cell damage.

Finally, a warning must be made about moving the electrode "in the plane of the retina". In order to facilitate fluid flow over the rabbit retina, the retina was mounted at a 30° angle from the horizontal. If the micromanipulator axes were not properly aligned, movements of the stimulating electrode might be misinterpreted. For example, Figure 5-4 depicts the case in which one of the micromanipulator axes - call it the y-axis - is aligned so that motion in the corresponding direction is parallel to the table. Since the retina is at an angle, moving the micromanipulator arm 50μm in the y direction corresponds to a somewhat larger displacement in the plane of the retina, as shown in the Figure.

5.3.4 Variations with time

When the retina is removed from the turtle or rabbit, its cells begin to die. In a typical experiment using a rabbit retina, stable light-evoked responses may be recorded many hours after removal of the retina. It was sometimes noted in experiments, however, that with all of the stimulus parameters held constant, thresholds increased significantly over the course of several minutes. The fact that thresholds varied over such a short time interval indicates that the properties of some element in the experimental apparatus are changing with time. The most likely candidates for such behavior are the electrode tip and the cell itself. The passage of current through the electrode will tend to corrode its surface to some extent. Furthermore, the health of the cell might be comprised by stimulation, either due to toxic byproducts produced at the electrode tip or from fatigue due to continuous stimulation. Corrosion and toxicity problems may be reduced through the use of biphasic, charge-balanced pulses [12]. In general, though, more control experiments need to be done

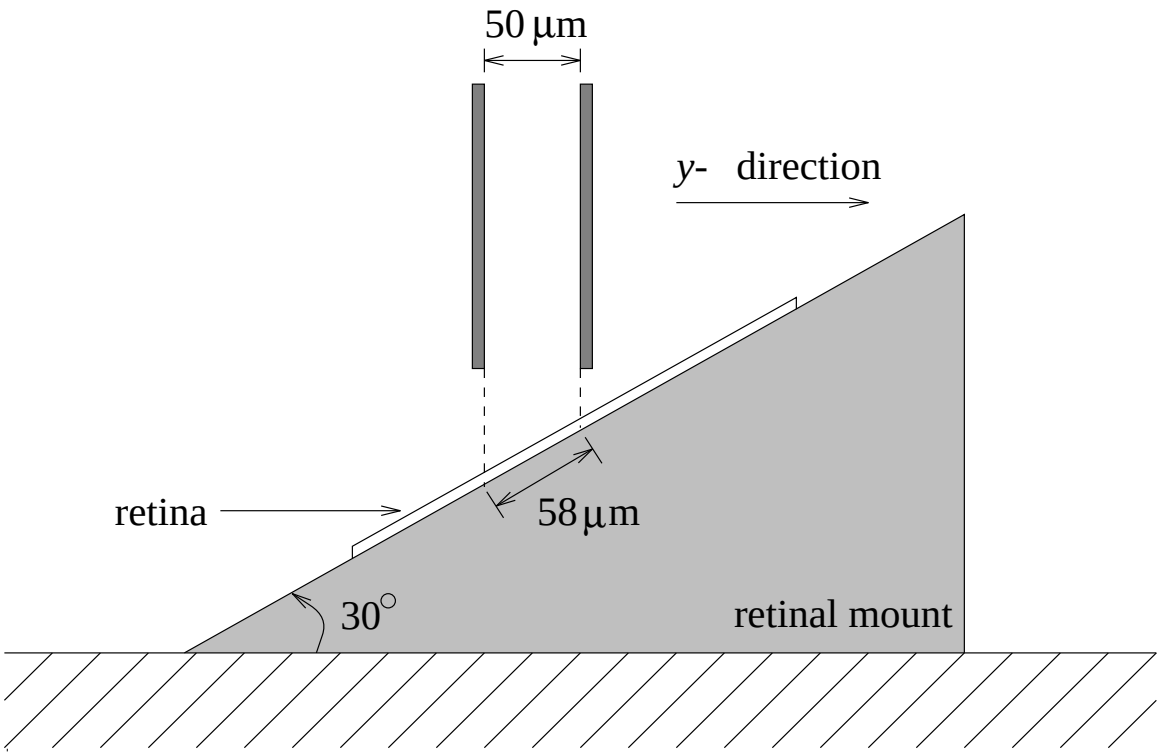

Figure 5-4: Movement of the stimulating electrode in a direction which is not parallel to the retina.

to investigate variations with time in our experimental apparatus.

Chapter 6

Conclusion

6.1 Summary

Through a discussion of the retina and of the retinal implant, Chapter 2 provided the relevant background material for the thesis. In this chapter, the anatomy and physiology of the retina were discussed, the motivation for and a functional description of the retinal implant were given, and the literature on electrical stimulation of retinal cells was reviewed. The chapter concluded with a formulation of the thesis problem. This problem was addressed in the following chapters using a combination of theoretical and experimental approaches. In Chapter 3 the theory of extracellular electrical stimulation was examined. Threshold comparisons were made based on the analysis of linear models of nerve cells in steady-state electric fields of fairly simple shape. The design and construction of a practical stimulating electrode, which we believe can be used for selective stimulation of ganglion cell bodies, is presented in Chapter 4. At the end of the chapter, a model for numerically predicting the electric fields produced by the electrode was presented. Finally, Chapter 5 describes the experiments that were performed to test three hypotheses stemming from the results of Chapter 3. For a number of reasons presented at the end of the chapter, these experiments yielded inconclusive results. The results themselves were not presented.

6.2 Suggestions for further study

Opportunities arose frequently during the course of this work to pursue some new line of inquiry, to refine the electrode design or construction, or to improve on our experimental methods. Many of these opportunities were not taken for one reason or another, and are therefore presented below as suggestions for future study.

6.2.1 Modeling and analysis

A number of fairly strong assumptions were made to facilitate the analysis of Chapter 3. A natural extension of this work would be to determine if any if these assumptions might be relaxed without making the problem analytically intractable. Some initial steps are taken to do this in appendices A and B, where the time-dependent responses of the linear cell models are examined. It was discovered in appendix A that the quasistatic models of the cell body and axon (in a transverse field) had time constants which were roughly a factor

of 1000 smaller than the membrane RC time constant. Additional thought should be given to the astonishing rapidity at which these models reach steady-state.

Other assumptions might be tackled numerically. Consider for instance the circuit model for the axon in a longitudinal field. To analyze the effects of a parallel-plate electrode on this model, we assumed that the axon itself did not play a role in determining the extracellular voltages. We would not expect this assumption to hold in a strict sense. To what extent would the axon model influence the extracellular electric field?

The problem amounts to solving Laplace's equation at the exterior surface of the model. In appendix A, a three-dimensional electroquasistic model for an unmyelinated axon was analyzed in a uniform, transverse electric field. Due to the symmetries of the model and of the stimulating field, analytical solutions for Laplace's equation could be found in a straightforward manner. Solutions which account for longitudinally nonuniform boundary conditions would be substantially more complex. Thus a numerical algorithm might be employed to find such solutions.

A second numerical problem was introduced at the end of Chapter 4. To predict the electric fields generated by the experimental stimulating electrode, a set of boundary conditions on Laplace's equation were established. A numerical algorithm has yet to be implemented to find the unique solution entailed by these boundary conditions.

6.2.2 Electrode construction

Three significant improvements can be made in the construction of single electrodes described in Chapter 4. First, the Clear 2-Ton epoxy (used to encapsulate the electrode and to cement it into the glass tube) leaves much to be desired. A harder-curing epoxy would be less susceptible to smearing during tip-grinding. When the 2-Ton epoxy smeared onto the electrode conductor surfaces, it might have changed their electrical properties, potentially altering the effective electrode geometry. Ideally the epoxy should not soften after prolonged exposure to salt water, either. Soft epoxy might be smeared over conductor surfaces in the course of electrode manipulation during an experiment. Again, this could lead to an alteration of the effective electrode geometry. Second, an alternative to glass needs to be found for the electrode housing. The glass capillary tubes were quite fragile and broke far too often. If a small metal tube (such as a hypodermic needle) is used, it will be necessary to insulate the conductor-insulator-conductor sandwich to circumvent stray shorts to the housing. Third, attempts could be made plate the electrode tip. Plating electrode tips using colloidal suspensions of gold or platinum black will lower the tip resistance, and possibly reduce the likelihood of tip corrosion and/or subsequent toxicity problems.

6.2.3 Experimental methods

If the experimental procedures described in Chapter 5 are to be continued, systematic attempts should be made to address each of the unresolved issues raised at the end of the chapter. More controls - and more experiments in general - need to be performed.

The problems with stimulus artifact encountered in the turtle preparation might be solved if the recording and stimulating electrodes could be placed further apart. Unfortunately, the size of the preparation is quite small to begin with (two to three millimeters in diameter), making this solution impractical. Given the constraint of a relatively small electrode separation, attempts might be made to minimize the amplitude and duration of the stimulus artifact. It was suggested in section 5.3, for example, that stimulus artifacts

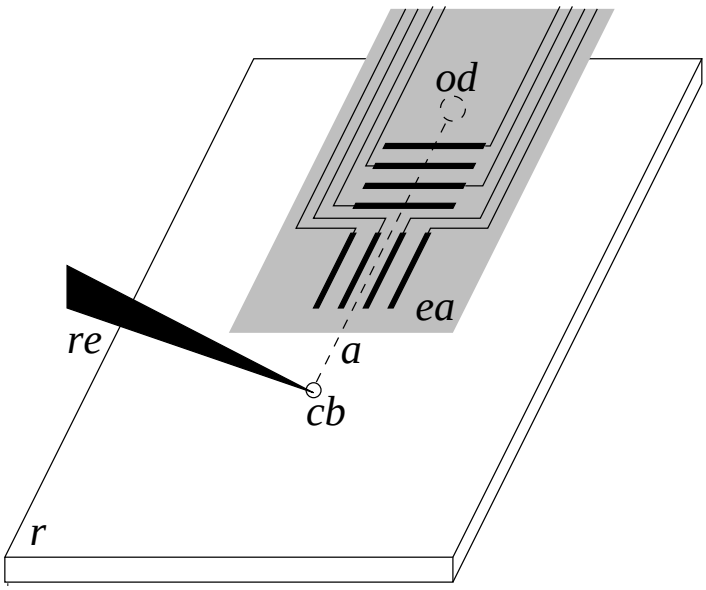

Figure 6-1: Stimulation of the retina with an electrode array (shaded). The thicker black lines on the array represent exposed conductor surfaces, while the thin lines represent wires which are insulated from the tissue. Abbreviations: *r* - retina; *a* - axon; *cb* - cell body; *od* - optic disk; *ea* - electrode array; *re* - recording electrode.

outlast stimulus pulses due to saturation of the recording amplifiers. If this is indeed the case, the duration of the artifacts might be minimized by disconnecting the leads of the recording electrode from the amplifiers during the application of stimulus pulses.

Other unresolved issues might be addressed successfully using an array of stimulating electrodes, such as that depicted in Figure 6-1. Rather than moving a stimulating electrode physically, the electrode could be moved "virtually" by connecting the stimulator across different pairs of conductors within the array. If the array is placed against the inner limiting membrane, variations in the electrode height above cells would be constrained to the biological variability of cell depth within the retina. This would remedy ambiguities of the sort illustrated in Figure 5-3. With the electrode free to move, the positions of cell bodies and axons might be deduced by plotting out thresholds obtained with the stimulating electrode in several different locations.

Appendix A

Additional mathematical derivations

A.1 Time dependent responses of cell body in a uniform field

Equations (3.3)-(3.8) describe a dynamic system. What type of response will it exhibit if the driving field $E_o(t)$ is not constant in time? In this section the time-dependent response of the plate/cell body system will be examined. This analysis will be directed at finding the time constants of the system and also on finding a circuit representation for the system dynamics.

In order to understand the time-dependent response of this system in terms of a circuit model, it is helpful to solve equations (3.3)-(3.8) in for the surface charge densities σ^i_{su} and σ^e_{su}. To do this it will be necessary to eliminate a, b, c, and d. First, solve for b and c in terms of a and d using equations (3.3) and (3.4).

$$\begin{aligned} b &= a - \frac{(R+\Delta)^3}{(R+\Delta)^3 - R^3}\left[a - \frac{d}{(R+\Delta)^3} + E_o(t)\right], \\ c &= \frac{(R+\Delta)^3 R^3}{(R+\Delta)^3 - R^3}\left[a - \frac{d}{(R+\Delta)^3} + E_o(t)\right]. \end{aligned}$$

Substitute these formulas for b and c into equations (3.5) and (3.6) and collect terms.

$$\begin{aligned} a\left[\epsilon_f + \epsilon_m \frac{2(R+\Delta)^3 + R^3}{(R+\Delta)^3 - R^3}\right] + \frac{d}{(R+\Delta)^3}\left[-\epsilon_m \frac{3(R+\Delta)^3}{(R+\Delta)^3 - R^3}\right] \\ = \frac{\sigma^i_{su}}{\cos\theta} + E_o(t)\left[-\epsilon_m \frac{3(R+\Delta)^3}{(R+\Delta)^3 - R^3}\right], \\ a\left[-\epsilon_m \frac{3R^3}{(R+\Delta)^3 - R^3}\right] + \frac{d}{(R+\Delta)^3}\left[2\epsilon_f + \epsilon_m \frac{(R+\Delta)^3 + 2R^3}{(R+\Delta)^3 - R^3}\right] \\ = \frac{\sigma^e_{su}}{\cos\theta} + E_o(t)\left[-\epsilon_f + \epsilon_m \frac{(R+\Delta)^3 + 2R^3}{(R+\Delta)^3 - R^3}\right]. \end{aligned}$$

The above equations can be greatly simplified by factoring a Δ out of the denominators,

$$(R+\Delta)^3 - R^3 = \Delta(3R^2 + 3R\Delta + \Delta^2),$$

noting the definition of membrane capacitance per unit area,

$$C_m = \epsilon_m/\Delta,$$

and using the approximation $\Delta \approx 0$ since $\Delta \ll R$. The results of the simplification are as follows.

$$a(\epsilon_f + C_m R) + d\left(\frac{-C_m}{R^2}\right) = \frac{\sigma^i_{su}}{\cos\theta} + E_o(t)(-C_m R), \tag{A.1}$$

$$a(-C_m R) + d\left(\frac{2\epsilon_f}{R^3} + \frac{C_m}{R^2}\right) = \frac{\sigma^e_{su}}{\cos\theta} + E_o(t)(-\epsilon_f + C_m R). \tag{A.2}$$

[Note in the above equations that if $\epsilon_f \ll C_m R$, $\sigma^i_{su} \approx -\sigma^e_{su}$ and we no longer have a second order system.]

b and c can be eliminated from equations (3.7) and (3.8) in a nearly identical manner, but this time using the definition of membrane conductance per unit area,

$$G_m = \sigma_m/\Delta.$$

The results are as follows

$$a(\sigma_i + G_m R) + d\left(-\frac{G_m}{R^2}\right) = -\frac{\dot{\sigma}^i_{su}}{\cos\theta} + E_o(t)(-G_m R), \tag{A.3}$$

$$a(-G_m R) + d\left(\frac{2\sigma_e}{R^3} + \frac{G_m}{R^2}\right) = -\frac{\dot{\sigma}^e_{su}}{\cos\theta} + E_o(t)(-\sigma_e + G_m R). \tag{A.4}$$

Now solve equations (A.3) and (A.4) for a and d. In matrix notation,

$$\begin{bmatrix} a \\ d \end{bmatrix} = -\left(\frac{R^3}{\cos\theta}\right) \frac{\begin{bmatrix} \frac{2\sigma_e}{R^3} + \frac{G_m}{R^2} & \frac{G_m}{R^2} \\ G_m R & \sigma_i + G_m R \end{bmatrix} \begin{bmatrix} \dot{\sigma}^i_{su} \\ \dot{\sigma}^e_{su} \end{bmatrix}}{2\sigma_i\sigma_e + 2\sigma_e G_m R + \sigma_i G_m R} + \frac{\begin{bmatrix} -\frac{3\sigma_e G_m}{R^2} \\ -\sigma_i\sigma_e \end{bmatrix} R^3 E_o(t)}{2\sigma_i\sigma_e + 2\sigma_e G_m R + \sigma_i G_m R}. \tag{A.5}$$

Substituting the above result into equations (A.1) and (A.2) yields the following ordinary differential equation in surface charge density.

$$-\frac{\begin{bmatrix} \epsilon_f + C_m R & -C_m R \\ -C_m R & 2\epsilon_f + C_m R \end{bmatrix} \begin{bmatrix} 2\sigma_e + G_m R & G_m R \\ G_m R & \sigma_i + G_m R \end{bmatrix} \begin{bmatrix} \dot{\sigma}^i_{su} \\ \dot{\sigma}^e_{su} \end{bmatrix}}{2\sigma_i\sigma_e + 2\sigma_e G_m R + \sigma_i G_m R} = \begin{bmatrix} \sigma^i_{su} \\ \sigma^e_{su} \end{bmatrix} + \begin{bmatrix} f_1 \\ f_2 \end{bmatrix} E_o(t)\cos\theta, \tag{A.6}$$

where

$$f_1 = \frac{3\epsilon_f\sigma_e G_m R + \sigma_e G_m C_m R^2 - \sigma_i C_m G_m R^2 - 3\sigma_i\sigma_e C_m R}{2\sigma_i\sigma_e + 2\sigma_e G_m R + \sigma_i G_m R}, \tag{A.7}$$

$$f_2 = \frac{-2\epsilon_f\sigma_e G_m R - \sigma_e G_m C_m R^2 + \sigma_i C_m G_m R^2 + 3\sigma_i\sigma_e C_m R - \epsilon_f\sigma_i G_m R}{2\sigma_i\sigma_e + 2\sigma_e G_m R + \sigma_i G_m R}. \tag{A.8}$$

Two important pieces of information come out of equation (A.6). The first is a circuit

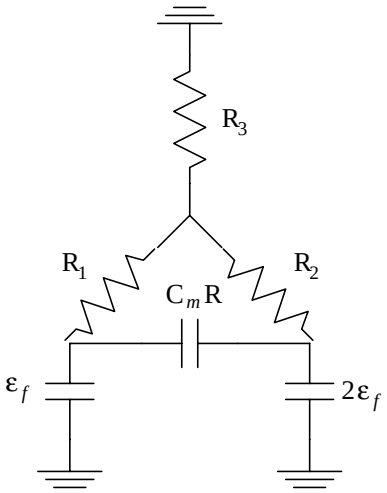

$$R_1 = \frac{2\,\sigma_e}{2\sigma_i\,\sigma_e + 2\sigma_e G_m R + \sigma_i\,G_m R}$$

$$R_2 = \frac{\sigma_i}{2\sigma_i\,\sigma_e + 2\sigma_e G_m R + \sigma_i\,G_m R}$$

$$R_3 = \frac{G_m R}{2\sigma_i\,\sigma_e + 2\sigma_e G_m R + \sigma_i\,G_m R}$$

Figure A-1: Circuit model for spherical cell.

representation of the nerve membrane dynamics. [not sorted out yet, but see Figure A-1].

The second important piece of information that can be obtained from equation (A.6) are the time constants of the system. The equation is of the general form

$$-A\,\dot{\mathbf{x}} = \mathbf{x} + \text{drive terms},$$

where A is a 2 by 2 matrix. The time constants of the system are simply the eigenvalues of the A matrix. Using the approximation that $\epsilon_f \ll C_m R$ to simplify things, it can be shown that

$$\tau = 0,\ \frac{C_m R(\sigma_i + 2\sigma_e)}{2\sigma_i\sigma_e + G_m R(\sigma_i + 2\sigma_e)}. \tag{A.9}$$

The zero-valued time constant is nonzero if the above approximation is not made. The zero-valued time constant represents a very fast equilibration of the two surface charge densities, σ^i_{su} and σ^e_{su}. The second time constant can be rewritten,

$$\frac{1}{\tau_2} = \frac{1}{R_m C_m} + \frac{2\sigma_i\sigma_e}{C_m R(\sigma_i + 2\sigma_e)}, \tag{A.10}$$

where

$$R_m = \frac{1}{G_m}$$

is the membrane sheet resistance. The first expression appearing on the right of equation (A.10) resembles a circuit RC time constant for the membrane. The second expression is determined by the membrane capacitance C_m but also by the radius of the cell R and the intracellular and extracellular conductivities σ_i and σ_e. To get an idea of the size of these quantities, we use the typical cell data listed in Table A.1. Also, the radius of a typical ganglion cell body is $R = 10^{-5}$m. Using these data,

$$\frac{1}{R_m C_m} = 10^3 \text{ s},$$

$R_m = 1000\Omega \cdot \text{cm}^2$	$C_m = 1 \times 10^{-6}\text{F/cm}^2$
$\sigma_e = 0.02$ S/cm	$\sigma_i = 0.005$ S/cm

Table A.1: Typical cell data. From Cartee and Plonsey (1992)

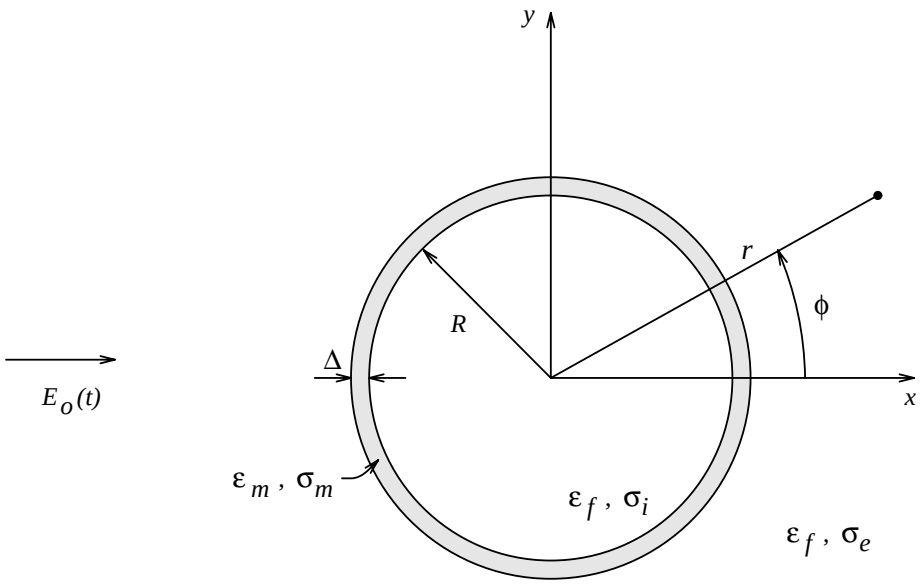

Figure A-2: Axon model.

$$\frac{2\sigma_i\sigma_e}{C_m R(\sigma_i + 2\sigma_e)} = 4.44 \times 10^6 \text{ s},$$

$$\tau_2 = 2.25 \times 10^{-7} \text{ s}.$$

In such a case, the second term dominates the τ_2, making it much smaller than the $R_m C_m$ product.

A.2 Axon in a uniform, transverse field

The same approach that was used to analyze the cell body in sections 3.2 and A.1 will now be applied to the axon.

A.2.1 Solution form and boundary conditions

An axon is modeled as an infinitely long cylindrical shell, as shown in Figure A-2.

The solution for the electric potential is of the form

$$\Phi = \begin{cases} a(t) r \cos\phi & \text{for } r < R, \\ b(t) r \cos\phi + \frac{c(t)}{r}\cos\phi & \text{for } R < r < R + \Delta, \\ -E_o(t) r \cos\phi + \frac{d(t)}{r}\cos\phi & \text{for } r > R + \Delta. \end{cases} \tag{A.11}$$

Before the boundary conditions for the problem are established, a couple of comments will be made about the solution form. First, for large r, the potential is approximately $-E_o(t)r\cos\phi$ or simply $-E_o(t)x$. This agrees with the previously established condition that the field is uniform and horizontally directed far from the cell. Second, note that there is no z-variation in the potential. This is due to the uniformly applied field and infinite length of the axon model. More importantly, it points to the relative simplicity of the solution, which for other applied fields and axon geometries would likely be a modal expansion in polar coordinates. Now we will establish the boundary conditions which apply to the solution given above.

The functions $a(t), b(t), c(t)$ and $d(t)$ can be related to each other and to the surface charge densities on the membrane:solution boundaries using continuity conditions established in subsection 3.2.1. Using the definition of electric potential, equation (3.2), the first of the three continuity conditions becomes

$$\frac{\partial \Phi^a}{\partial \phi} = \frac{\partial \Phi^b}{\partial \phi}.$$

The remaining two continuity conditions simplify to

$$-\epsilon_a \frac{\partial \Phi^a}{\partial r} + \epsilon_b \frac{\partial \Phi^b}{\partial r} = \sigma_{su},$$

$$-\sigma_a \frac{\partial \Phi^a}{\partial r} + \sigma_b \frac{\partial \Phi^b}{\partial r} = -\dot{\sigma}_{su},$$

as before. Note that in this Section r represents the polar coordinate radius as defined in Figure (A-2), whereas in the previous section r represented the spherical coordinate radius as defined in Figure (3-3).

Application of the continuity conditions at $r = R$ and $r = R + \Delta$ yield the following equations.

$$bR + \frac{c}{R} = aR, \tag{A.12}$$

$$-E_o(t)(R+\Delta) + \frac{d}{R+\Delta} = b(R+\Delta) + \frac{c}{R+\Delta}, \tag{A.13}$$

$$-\epsilon_m \left(b - \frac{c}{R^2}\right)\cos\phi + \epsilon_f a \cos\phi = \sigma^i_{su}, \tag{A.14}$$

$$-\epsilon_f \left[-E_o(t) - \frac{d}{(R+\Delta)^2}\right]\cos\phi + \epsilon_m \left[b - \frac{c}{(R+\Delta)^2}\right]\cos\phi = \sigma^e_{su}, \tag{A.15}$$

$$-\sigma_m \left(b - \frac{c}{R^2}\right)\cos\phi + \sigma_i a \cos\phi = -\dot{\sigma}^i_{su}, \tag{A.16}$$

$$-\sigma_e \left[-E_o(t) - \frac{d}{(R+\Delta)^2}\right]\cos\phi + \sigma_m \left[b - \frac{c}{(R+\Delta)^2}\right]\cos\phi = -\dot{\sigma}^e_{su}\,. \tag{A.17}$$

In the above equations, $a = a(t)$, $b = b(t)$, $c = c(t)$, $d = d(t)$, and σ^i_{su} and σ^e_{su} are the surface charge densities on the intracellular and extracellular membrane:solution boundaries, respectively. These equations completely describe a linear time-invariant system

in six variables (a, b, c, d, σ^i_{su}, and σ^e_{su}) which can be solved completely for a given $E_o(t)$.

A.2.2 Time-independent solution

If the applied field is held constant at E_o, and the system described above is in steady state, the time derivatives in equations (A.16) and (A.17) will be zero. In such a case, equations (A.12),(A.13), (A.16), and (A.17) can be solved for a, b, c, and d.

From equations (A.12) and (A.13), it can be shown that

$$b = a - \frac{(R+\Delta)^2}{(R+\Delta)^2 - R^2}\left[a - \frac{d}{(R+\Delta)^2} + E_o\right], \tag{A.18}$$

$$c = \frac{(R+\Delta)^2 R^2}{(R+\Delta)^2 - R^2}\left[a - \frac{d}{(R+\Delta)^2} + E_o\right]. \tag{A.19}$$

Substituting into equations (A.16) and (A.17), noting that the time derivatives are zero, and collecting terms yields

$$a\left[\sigma_i+\sigma_m\frac{(R+\Delta)^2+R^2}{(R+\Delta)^2-R^2}\right]+\frac{d}{(R+\Delta)^2}\left[-\sigma_m\frac{2(R+\Delta)^2}{(R+\Delta)^2-R^2}\right]=E_o\left[-\sigma_m\frac{2(R+\Delta)^2}{(R+\Delta)^2-R^2}\right],$$

$$a\left[-\sigma_m\frac{2R^2}{(R+\Delta)^2-R^2}\right]+\frac{d}{(R+\Delta)^2}\left[\sigma_e+\sigma_m\frac{(R+\Delta)^2+R^2}{(R+\Delta)^2-R^2}\right]=E_o\left[-\sigma_e+\sigma_m\frac{(R+\Delta)^2+R^2}{(R+\Delta)^2-R^2}\right].$$

Several of the expressions in the two preceding equations can be written in terms of the membrane conductance per unit area defined in equation (3.11) by noting that

$$\frac{\sigma_m}{(R+\Delta)^2 - R^2} = \frac{G_m}{2R+\Delta}.$$

After making this substitution, we have

$$a\left[\sigma_i+G_m\frac{(R+\Delta)^2+R^2}{2R+\Delta}\right]+\frac{d}{(R+\Delta)^2}\left[-G_m\frac{2(R+\Delta)^2}{2R+\Delta}\right]=E_o\left[-G_m\frac{2(R+\Delta)^2}{2R+\Delta}\right],$$

$$a\left[-G_m\frac{2R^2}{2R+\Delta}\right]+\frac{d}{(R+\Delta)^2}\left[\sigma_e+G_m\frac{(R+\Delta)^2+R^2}{2R+\Delta}\right]=E_o\left[-\sigma_e+G_m\frac{(R+\Delta)^2+R^2}{2R+\Delta}\right].$$

The equations that have been derived thus far can now be greatly simplified by recognizing that membrane thickness Δ is much less than the axon radius R. Specifically, cell membranes thickness is on the order of 75Å, whereas the radius of a typical axon is roughly 0.5μm[26]. Thus the axon radius is almost 100 times greater than the cell membrane thickness. Based on this comparison, we make the approximation $\Delta \approx 0$ to obtain

$$a(\sigma_i + G_m R) + d\left(-\frac{G_m}{R}\right) = E_o(-G_m R),$$

$$a(-G_m R) + d\left(\frac{\sigma_e}{R^2} + \frac{G_m}{R}\right) = E_o(-\sigma_e + G_m R).$$

Now a and d can be found fairly easily, and are given by

$$a = -\frac{2\sigma_e G_m R}{\sigma_i G_m R + \sigma_e G_m R + \sigma_i \sigma_e} E_o, \tag{A.20}$$

$$d = \frac{\sigma_i G_m R^3 - \sigma_e G_m R^3 - \sigma_i \sigma_e R^2}{\sigma_i G_m R + \sigma_e G_m R + \sigma_i \sigma_e} E_o. \tag{A.21}$$

Equations (A.11), (A.20) and (A.21) provide a complete solution for the electric potential inside and outside of the axon model. To determine the potential inside of the cell membrane, it would be necessary to find b and c. This could be done by substituting the solutions for a and d back into equations (A.18) and (A.19). As in the case of the cell body model, however, the potential inside the membrane is not of critical importance, so we will neglect b and c altogether.

Applying the definition of transmembrane potential given in equation (3.14) to the solution above gives

$$\boxed{V_m = \frac{2\sigma_i \sigma_e R}{\sigma_i G_m R + \sigma_e G_m R + \sigma_i \sigma_e} E_o \cos\phi.} \tag{A.22}$$

Note the similarity between the induced transmembrane potential for the cylindrical and spherical models. All of the major points made in Subsection 3.2.3 apply to the cylindrical axon model.

A.2.3 Time-dependent solutions

In this section the system dynamics of equations (A.12)-(A.17) are examined. The derivations parallel those used for the spherical cell.

The four coefficients a, b, c and d may be eliminated from equations (A.12)-(A.17), leaving an ordinary differential equation in the surface charge densities, σ^i_{su} and σ^e_{su}. Solve for b and c in terms of a and d using equations (A.12) and (A.13).

$$\begin{aligned} b &= a - \frac{(R+\Delta)^2}{(R+\Delta)^2 - R^2}\left[a - \frac{d}{(R+\Delta)^2} + E_o(t)\right], \\ c &= \frac{(R+\Delta)^2 R^2}{(R+\Delta)^2 - R^2}\left[a - \frac{d}{(R+\Delta)^2} + E_o(t)\right]. \end{aligned}$$

Substitute formulas for b and c into equations (A.14) and (A.15) and collect terms.

$$\begin{aligned} a\left[\epsilon_f + \epsilon_m \frac{(R+\Delta)^2 + R^2}{(R+\Delta)^2 - R^2}\right] + \frac{d}{(R+\Delta)^2}\left[-\epsilon_m \frac{2(R+\Delta)^2}{(R+\Delta)^2 - R^2}\right] \\ = \frac{\sigma^i_{su}}{\cos\phi} + E_o(t)\left[-\epsilon_m \frac{2(R+\Delta)^2}{(R+\Delta)^2 - R^2}\right], \\ a\left[-\epsilon_m \frac{2R^2}{(R+\Delta)^2 - R^2}\right] + \frac{d}{(R+\Delta)^2}\left[\epsilon_f + \epsilon_m \frac{(R+\Delta)^2 + R^2}{(R+\Delta)^2 - R^2}\right] \\ = \frac{\sigma^e_{su}}{\cos\phi} + E_o(t)\left[-\epsilon_f + \epsilon_m \frac{(R+\Delta)^2 + R^2}{(R+\Delta)^2 - R^2}\right]. \end{aligned}$$

Factor a Δ out of the denominators,

$$(R+\Delta)^2 - R^2 = \Delta(2R + \Delta),$$

make use of the definition of membrane capacitance per unit area, $C_m = \epsilon_m/\Delta$, and ap-

proximate $\Delta \approx 0$ since $\Delta \ll R$.

$$a(\epsilon_f + C_m R) + d\left(-\frac{C_m}{R}\right) = \frac{\sigma^i_{su}}{\cos\phi} + E_o(t)(-C_m R), \tag{A.23}$$

$$a(-C_m R) + d\left(\frac{\epsilon_f}{R^2} + \frac{C_m}{R}\right) = \frac{\sigma^e_{su}}{\cos\phi} + E_o(t)(-\epsilon_f + C_m R). \tag{A.24}$$

[Note in the above equations that if $\epsilon_f \ll C_m R$, $\sigma^i_{su} \approx -\sigma^e_{su}$ and we no longer have a second order system.]

b and c may be eliminated from equations (A.16) and (A.17) in a nearly identical manner, but this time using the definition of membrane conductance per unit area, $G_m = \sigma_m/\Delta$. Derivations yield

$$a(\sigma_i + G_m R) + d\left(-\frac{G_m}{R}\right) = \frac{-\dot{\sigma}^i_{su}}{\cos\phi} + E_o(t)(-G_m R), \tag{A.25}$$

$$a(-G_m R) + d\left(\frac{\sigma_e}{R^2} + \frac{G_m}{R}\right) = \frac{-\dot{\sigma}^e_{su}}{\cos\phi} + E_o(t)(-\sigma_e + G_m R). \tag{A.26}$$

Now solve equations (A.25) and (A.26) for a and d. In matrix notation,

$$\begin{bmatrix} a \\ d \end{bmatrix} = \left(\frac{-R^2}{\cos\phi}\right) \frac{\begin{bmatrix} \frac{\sigma_e}{R^2} + \frac{G_m}{R} & \frac{G_m}{R} \\ G_m R & \sigma_i + G_m R \end{bmatrix} \begin{bmatrix} \dot{\sigma}^i_{su} \\ \dot{\sigma}^e_{su} \end{bmatrix}}{\sigma_i\sigma_e + \sigma_i G_m R + \sigma_e G_m R} + \frac{\begin{bmatrix} \frac{-2\sigma_e G_m}{R} \\ -\sigma_i\sigma_e \end{bmatrix} R^2 E_o(t)}{\sigma_i\sigma_e + \sigma_i G_m R + \sigma_e G_m R}. \tag{A.27}$$

Substituting the above results into equations (A.23) and (A.24) yields the following ordinary differential equation in surface charge density.

$$-\frac{\begin{bmatrix} \epsilon_f + C_m R & -C_m R \\ -C_m R & \epsilon_f + C_m R \end{bmatrix} \begin{bmatrix} \sigma_e + G_m R & G_m R \\ G_m R & \sigma_i + G_m R \end{bmatrix} \begin{bmatrix} \dot{\sigma}^i_{su} \\ \dot{\sigma}^e_{su} \end{bmatrix}}{\sigma_i\sigma_e + \sigma_i G_m R + \sigma_e G_m R} = \begin{bmatrix} \sigma^i_{su} \\ \sigma^e_{su} \end{bmatrix} + \begin{bmatrix} f_1 \\ f_2 \end{bmatrix} E_o(t)\cos\phi, \tag{A.28}$$

where

$$f_1 = \frac{2\epsilon_f\sigma_e G_m R + \sigma_e C_m G_m R^2 - \sigma_i C_m G_m R^2 - 2\sigma_i\sigma_e C_m R}{\sigma_i\sigma_e + \sigma_i G_m R + \sigma_e G_m R}, \tag{A.29}$$

$$f_2 = \frac{-\epsilon_f\sigma_e G_m R - \sigma_e C_m G_m R^2 + \sigma_i C_m G_m R^2 + 2\sigma_i\sigma_e C_m R - \epsilon_f\sigma_i G_m R}{\sigma_i\sigma_e + \sigma_i G_m R + \sigma_e G_m R}. \tag{A.30}$$

As in the case of the sphere, two important pieces of information can be found in equation (A.28); a circuit representation of the system and the system time constants. The circuit representation is shown in Figure A-3. Its topology is identical to that of the sphere, but the resistor values are slightly different. Also, the cylinder radius R is somewhat smaller than that of the sphere.

To find the time constants of the system, note again that equation (A.28) is of the form

$$-A\,\dot{\mathbf{x}} = \mathbf{x} + \text{drive terms}.$$

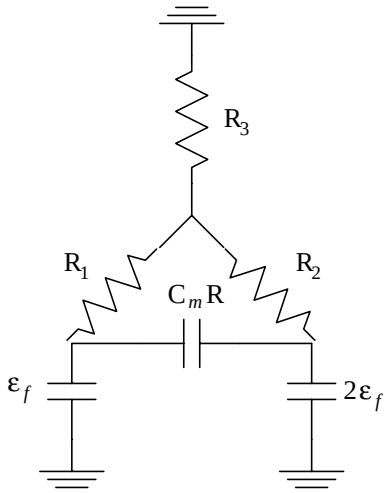

$$R_1 = \frac{\sigma_e}{\sigma_i \sigma_e + \sigma_e G_m R + \sigma_i G_m R}$$

$$R_2 = \frac{\sigma_i}{\sigma_i \sigma_e + \sigma_e G_m R + \sigma_i G_m R}$$

$$R_3 = \frac{G_m R}{\sigma_i \sigma_e + \sigma_e G_m R + \sigma_i G_m R}$$

Figure A-3: Circuit model for cylindrical cell.

The time constants of the system are the eigenvalues of the A matrix. Using the fact that $\epsilon_f \ll C_m R$, the time constants are found to be

$$\tau = 0, \ \frac{C_m R(\sigma_i + \sigma_e)}{\sigma_i \sigma_e + G_m R(\sigma_i + \sigma_e)}. \tag{A.31}$$

The zero-valued time constant arises because the approximation $\epsilon_f \approx 0$ was made. The second time constant can be rewritten

$$\frac{1}{\tau_2} = \frac{1}{R_m C_m} + \frac{\sigma_i \sigma_e}{C_m R(\sigma_i + \sigma_e)}. \tag{A.32}$$

The first expression appearing on the right of equation (A.32) resembles a circuit RC time constant for the membrane. The second expression, as in the case of the sphere, is determined by the membrane capacitance C_m, the radius of the cell R and the intracellular and extracellular conductivities σ_i and σ_e. Again the time constant will be dominated by the second expression. Since the axon radius $R \approx 5 \times 10^{-7}$m is somewhat smaller than that of the sphere, the time constant for the axon will be somewhat smaller than that of the sphere. Using the data of Table A.1,

$$\frac{1}{R_m C_m} = 10^3 \text{ s},$$

$$\frac{\sigma_i \sigma_e}{C_m R(\sigma_i + \sigma_e)} = 8 \times 10^9 \text{ s},$$

$$\tau_2 = 1.25 \times 10^{-8} \text{ s}.$$

Appendix B

SPICE simulation of axon in longitudinal field

To examine the time-dependent behavior of the model for an axon in a longitudinal field, a SPICE simulation was run on the circuit of Figure B-1. An abbreviated version of the input file is given at the end of this appendix.

B.1 Circuit description

A small unit of axonal length Δ is represented by the circuit block in the dashed enclosure. Using the notation of section 3.3, we see from the Figure that

$$c_m = \frac{1\text{mF}}{\Delta},$$

$$g_m = \frac{1/1\Omega}{\Delta},$$

$$r_i = \frac{0.01\Omega}{\Delta}.$$

From equation (3.20),

$$\lambda_c = \sqrt{\frac{\Delta^2}{(1/1\Omega)(0.01\Omega)}} = 10\Delta,$$

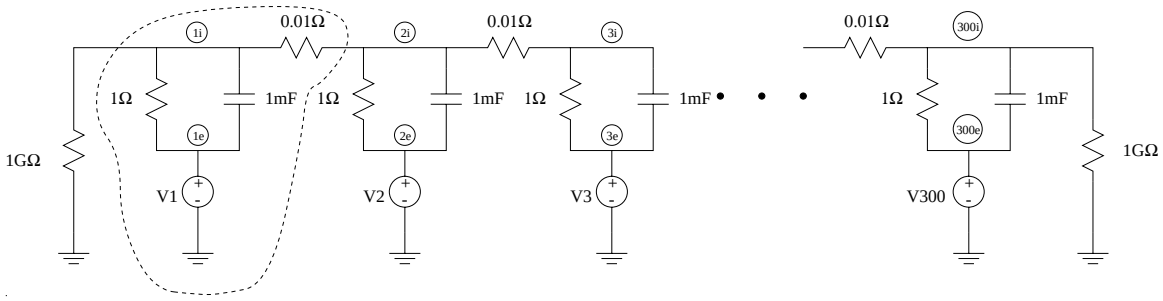

Figure B-1: SPICE simulation circuit for axon in a longitudinal field.

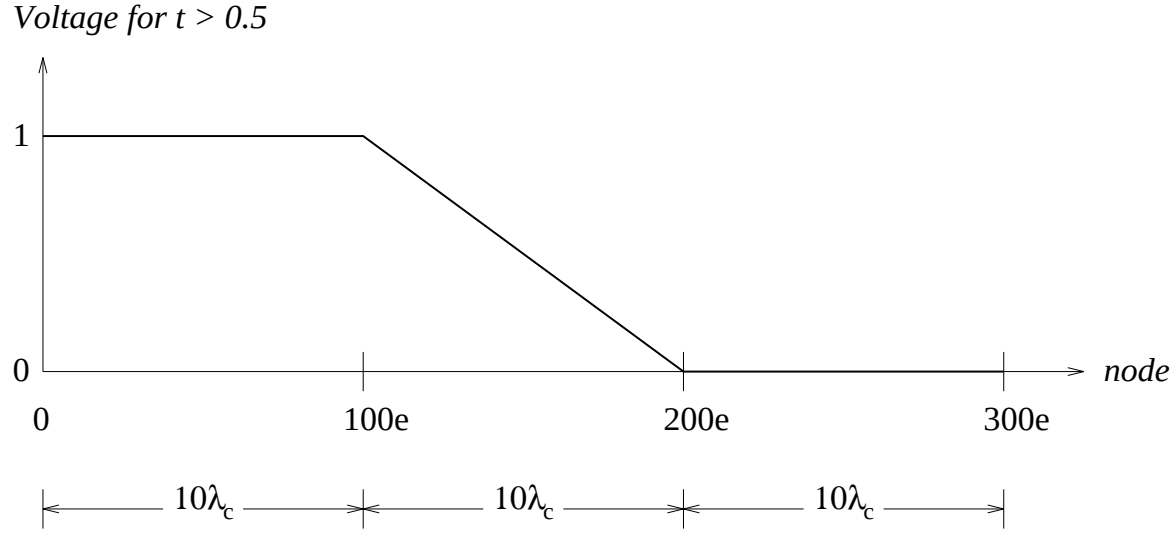

Figure B-2: Distribution of source voltages along the axon model circuit.

Thus, the circuit of Figure B-1 represents an axon which is $300\Delta = 30\lambda_c$ long. From equation (3.21),

$$\tau_m = \frac{0.001\text{F}}{1/1\Omega} = 1\text{ms}.$$

This is the same as the membrane RC time constant found in section A.1.

The circled numbers in Figure B-1 represent the nodes of the circuit model between each of the length-Δ segments. Nodes 1i-300i represent intracellular voltages of the circuit model, and nodes 1e-300e represent the extracellular voltages at corresponding locations. Applied extracellular voltages are modeled with perfect voltage sources V1-V300. To find the step response of the circuit, the voltages were initially set to zero. For $t > 0.5$ms the voltage sources were assigned as in Figure B-2. Note that segments of length $10\lambda_c$ surround the two breakpoints at nodes 100e and 200e. These breakpoints represent impulses in the activating function (see section 3.3), and were intentionally placed "far away" from each other and from the left and right boundaries of the circuit.

B.2 Results

Plotted in Figure B-3 is the intracellular voltage at several nodes in the rightmost portion of the circuit. Since the extracellular voltage at these locations is zero, the intracellular voltage is equal to the induced transmembrane potential. The solid line, which represents the transmembrane potential at one of the breakpoints, rises fastest. The dotted vertical and horizontal lines indicate that this quantity reaches 63% of its final value at

$$\tau = 0.4\text{ms}$$

after the extracellular voltages are switched on. Note that *this interval is less than the membrane RC time constant*. Further away from the breakpoint, the intracellular voltages rise more slowly and attain lower final values.

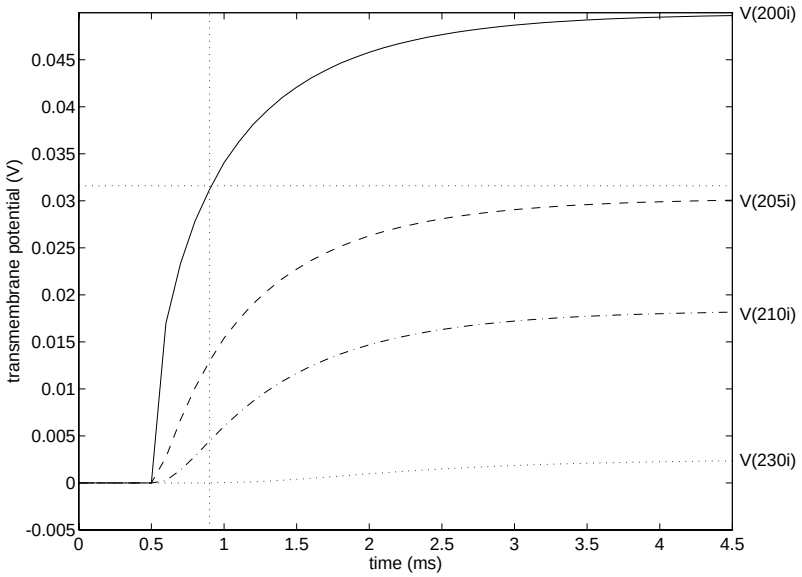

Figure B-3: "Intracellular" voltage vs. time.

B.3 Abbreviated SPICE input file

```
* ladder network

.subckt ladder 1 2 3
r1 1 2 0.01
r2 2 3 1
c1 2 3 0.001
.ends

*** rc ladder network

*** left side
r1 1000 0 1G * terminate with large resistance to ground
x1 1000 1 vl ladder
x2 1 2 vl ladder
x3 2 3 vl ladder
.
.
.
x98 97 98 vl ladder
x99 98 99 vl ladder
x100 99 100 vl ladder

vleft vl 0 dc 0 pulse(0 1 0.5m 2u 2u 10m 20m)

*** middle
```

```
x101 100 101 500 ladder
x102 101 102 501 ladder
x103 102 103 502 ladder
.
.
.
x197 196 197 596 ladder
x198 197 198 597 ladder
x199 198 199 598 ladder
x200 199 200 599 ladder

e101 500 0 (vl,0) 0.990000
e102 501 0 (vl,0) 0.980000
e103 502 0 (vl,0) 0.970000
.
.
.
e198 597 0 (vl,0) 0.020000
e199 598 0 (vl,0) 0.010000
e200 599 0 (vl,0) 0.000000


*** right side
x201 200 201 0 ladder
x202 201 202 0 ladder
x203 202 203 0 ladder
.
.
.
x298 297 298 0 ladder
x299 298 299 0 ladder
x300 299 1001 0 ladder
r2 1001 0 1G * terminate with large resistor
***
.op
.tran 0.1m 10m
.print tran v(200) v(205) v(210) v(230)
.options nomod ingold=2 numdgt=8 post
.end
```

References

[1] F.R. Amthor, C.W. Oyster, and E.S. Takahashi. Quantitative morphology of rabbit retinal ganglion cells. *Proc. R. Soc. Lond. B*, 217, 1983.

[2] A. Benjamin, M. Humayun, D. Hickingbotham, E. de Juan, Jr., and C. van den Honert. Characterization of retinal responses to electrical stimulation of retinal surface of rana catesbeiana. *Investigative Opthalmology and Visual Science*, 35(4):1832, March 15 1994. ARVO abstract.

[3] E. Berson. Retinitis pigmentosa. *Investigative Opthalmology and Visual Science*, 34(5):1659–1676, April 1993.

[4] L. Borg-Graham. On directional selectivity in vertebrate retina: An experimental and computational study. Technical Report 1350, MIT Artificial Intelligence Laboratory, 1992.

[5] R. Brancato, R. Pratesi, G. Leoni, G. Trabucchi, and U. Vanni. Histopathology of diode and argon laser lesions in rabbit retina: a comparative study. *Investigative Opthalmology and Visual Science*, 30(7):1504–1510, July 1989.

[6] G.S. Brindley. The site of electrical excitation of the human eye. *Journal of Physiology*, 127:189–200, 1955.

[7] Peter Carras, Paul Coleman, and Robert Miller. Site of action potential initiation in amphibian retinal ganglion cells. *Journal of Neurophysiology*, 67(2):292–304, February 1992.

[8] L. Cartee and R. Plonsey. The transient subthreshold response of spherical and cylindrical cell models to extracellular stimulation. *IEEE Transactions on Biomedical Engineering*, 39(1):76–85, January 1992.

[9] P. Coleman and R. Miller. Measurement of passive membrane parameters with whole-cell recording from neurons in the intact amphibian retina. *Journal of Neurophysiology*, 61(1):218–230, January 1989.

[10] D. Crapper and W. Noell. Retinal excitation and inhibition from direct electrical stimulation. *Journal of Neurophysiology*, 26:924–947, 1963.

[11] W. Dawson and N. Radtke. The electrical stimulation of the retina by indwelling electrodes. *Investigative Opthalmology and Visual Science*, 16(3):249–252, March 1977.

[12] J. M. R. Delgado. Electrodes for extracellular stimulation and recording. In W.L. Nastuk, editor, *Physical Techniques in Biological Research*, volume V: Electrophysiological Methods, Part A. Academic Press, 1964.

[13] R. Doty and F. Grimm. Cortical responses to local electrical stimulation of retina. *Experimental Neurology*, 5:319–334, 1962.

[14] J. Dowling. *The Retina: An Approachable Part of the Brain*. The Belknap Press of Harvard University Press, 1987.

[15] J. Dowling and B. Boycott. Retinal ganglion cells: A correlation of anatomical and physiological approaches. In B. Straatsma, M. Hall, R. Allen, and F. Crescitelli, editors, *The Retina: Morphology, Function, and Clinical Characteristics*. University of California Press, 1969.

[16] C.D. Ferris. *Introduction to Bioelectrodes*. Plenum Press, 1974.

[17] K. Frank and M. Becker. Microelectrodes for recording and stimulation. In W.L. Nastuk, editor, *Physical Techniques in Biological Research*, volume V: Electrophysiological Methods, Part A. Academic Press, 1964.

[18] B. Gernandt and R. Granit. Single fibre analysis of inhibition and the polarity of the retinal elements. *Journal of Neurophysiology*, 10:295–302, 1947.

[19] R. Granit. The distribution of excitation and inhibition in single-fibre responses from a polarized retina. *Journal of Physiology*, 105:45–53, 1946.

[20] R. Granit. Neural organization of the retinal elements, as revealed by polarization. *Journal of Neurophysiology*, 11:239–251, 1948.

[21] A.L. Hodgkin and A.F. Huxley. A quantitative description of membrane current and its application to conduction and excitation in nerve. *Journal of Physiology*, 117:500–544, 1952.

[22] A.L. Hodgkin and W.A.H. Rushton. The electrical constants of a crustacean nerve fiber. *Proc. Roy. Soc. Lond. B.*, 133:444–479, 1946.

[23] C. Howarth. Strength duration curves for electrical stimulation of the human eye. *The Quarterly Journal of Experimental Psychology*, 6:47–61, 1954.

[24] M. Humayun, R. Propst, E. de Juan, Jr., K. McCormick, and D. Hickingbotham. Bipolar surface electrical stimulation of the vertebrate retina. *Archives of Opthalmology*, 112:110–116, January 1994.

[25] M.S. Humayun, R.H. Propst, D. Hickingbotham, E. de Juan, Jr., and G. Dagnelie. Visual sensations produced by electrical stimulation of the retinal surface in patients with end-stage retinitis-pigmentosa. *Investigative Opthalmology and Visual Science*, 34(4):834, March 15 1993. ARVO abstract.

[26] R. Jensen. Personal communication.

[27] R. Jensen. Mechanism and site of action of a dopamine D1 antagonist in the rabbit retina. *Visual Neuroscience*, 3:573–585, 1989.

[28] R. Jensen. Intracellular recording of light responsees from visually identified ganglion cells in the rabbit retina. *Journal of Neuroscience Methods*, 40:101–112, 1991.

[29] R. Knighton. An electrically evoked slow potential of the frog's retina. I. properties of response. *Journal of Neurophysiology*, 38:185–197, 1975.

[30] R. Knighton. An electrically evoked slow potential of the frog's retina. II. identification with PII component of electroretinogram. *Journal of Neurophysiology*, 38:198–209, 1975.

[31] S. Kuffler. Discharge patterns and functional organization of mammalian retina. *Journal of Neurophysiology*, 16:37–68, 1953.

[32] S. Kuffler, J. Nicholls, and A. Martin. *From Neuron to Brain: A Cellular Approach to the Function of the Nervous System*. Sinauer Associates Inc., 1984.

[33] D.R. McNeal. Analysis of a model for excitation of myelinated nerve. *IEEE Transactions on Biomedical Engineering*, 23(4):329–337, July 1976.

[34] M. Meister, J. Pine, and D. Baylor. Multi-neuronal signals from the retina: acquisition and analysis. *Journal of Neuroscience Methods*, 51:95–106, 1994.

[35] S. Molotchnikoff. Transient responses of rabbit retinal ganglion cells to photic and electrical stimuli. *The Canadian Journal of Neurological Sciences*, pages 73–79, February 1976.

[36] S. Molotchnikoff. Lateral geniculate cell responses to electrical stimulation of the retina. *Brain Research*, 152:81–95, 1978.

[37] K. Motokawa. Retinal processes and their role in color vision. *Journal of Neurophysiology*, 12(5):291–303, September 1949.

[38] M. Narayanan, J. Rizzo, D. Edell, and J. Wyatt. Development of a silicon retinal implant: cortical evoked potentials following stimulation of the rabbit retina with light and electricity. *Investigative Opthalmology and Visual Science*, 35(4):1380, March 15 1994. ARVO abstract.

[39] T. Ogden and K. Brown. Intraretinal responses of the cynamolgus monkey to electrical stimulation of the optic nerve and retina. *Journal of Neurophysiology*, 27:682–705, 1964.

[40] R. Pagon. Retinitis pigmentosa. *Survey of Opthalmology*, 33(3):137–177, November-December 1988.

[41] R. Plonsey and K. Altman. Electrical stimulation of excitable cells - a model approach. *Proceedings of the IEEE*, 76(9):1122–1128, September 1988.

[42] S. Polyak. *The Retina*. The University of Chicago Press, 1941.

[43] A. Potts and J. Inoue. The electrically evoked resonse (EER) of the visual system. ii. effect of adaptation and retinitis pigmentosa. *Investigative Opthalmology and Visual Science*, 8(6):605–612, December 1969.

[44] A. Potts, J. Inoue, and D. Buffum. The electrically evoked resonse of the visual system (EER). *Investigative Opthalmology and Visual Science*, 7(3):269–278, June 1968.

[45] James B. Ranck, Jr. Which elements are excited in electrical stimulation of mammalian central nervous system: a review. *Brain Research*, 98:417–440, 1975.

[46] James B. Ranck, Jr. Extracellular stimulation. In M. Patterson and R. Kesner, editors, *Electrical Stimulation Research Techniques*. Academic Press, 1981.

[47] Frank Rattay. Analysis of models for external stimulation of axons. *IEEE Transactions on Biomedical Engineering*, BME-33(10):974–977, October 1986.

[48] Frank Rattay. Analysis of models for extracellular fiber stimulation. *IEEE Transactions on Biomedical Engineering*, 36(7):676–682, July 1989.

[49] J. Rizzo. Personal communication.

[50] L.S. Robblee and T.L. Rose. The electrochemistry of electrical stimulation. *Annual International Conference of the IEEE Engineering in Medicine and Biology Society*, 12(4):1479–80, 1990.

[51] J.T. Rubinstein. Analytical theory for extracellular electrical stimulation of nerve with focal electrodes. II. passive myelinated axon. *Biophysical Journal*, 60:538–555, September 1991.

[52] J.T. Rubinstein and F.A. Spelman. Analytical theory for extracellular electrical stimulation of nerve with focal electrodes. I. passive unmyelinated axon. *Biophysical Journal*, 54:975–981, December 1988.

[53] W.A.H. Rushton. The effect upon the threshold for nervous excitation of the length of nerve exposed, and the angle between current and nerve. *Journal of Physiology*, 63:357–377, 1927.

[54] P. Schiller. The on and off channels of the visual system. *Trends in Neurosciences*, 15(3):86–92, 1992.

[55] P. Schiller and N. Logothetis. The color-opponent and broad-band channels of the primate visual system. *Trends in Neurosciences*, 13(10):392–398, 1990.

[56] H.P. Schwan. Determination of biological impedances. In W.L. Nastuk, editor, *Physical Techniques in Biological Research*, volume VI: Electrophysiological Methods, Part B. Academic Press, 1963.

[57] W. Smiddy and E. Hernandez. Histopathologic results of retinal diode laser photocoagulation in rabbit eyes. *Archives of Opthalmology*, 110:693–698, May 1992.

[58] K. Spiegler and M. Wyllie. Electric potential differences. In G. Oster and A. Pollister, editors, *Physical Techniques in Biological Research*, volume II: Physical Chemical Techniques. Academic Press, 1956.

[59] J. Stone. *Parallel Processing in the Visual System*. Plenum Press, 1983.

[60] J. Stone, W. Barlow, M. Humayun, E. de Juan, Jr., and A. Milam. Morphometric analysis of macular photoreceptors and ganglion cells in retinas with retinitis pigmentosa. *Archives of Opthalmology*, 110:1634–1639, November 1992.

[61] E.N. Warman, W.M. Grill, and D. Durand. Modeling the effects of electric fields on nerve fibers: Determination of excitation thresholds. *IEEE Transactions on Biomedical Engineering*, 39(12):1244–1254, December 1992.

[62] H. Wässle and B. Boycott. Functional architecture of the mammalian retina. *Physiological Reviews*, 71(2):447–480, April 1991.

[63] T.F. Weiss. *A Textbook of Cellular Physiology and Biophysics.* MIT 6.021J Course Notes, 1992.

[64] J. Wyatt, J. Rizzo, A. Grumet, D. Edell, and R. Jensen. Development of a silicon retinal implant: epiretinal stimulation of retinal ganglion cells in the rabbit. *Investigative Opthalmology and Visual Science*, 35(4):1380, March 15 1994. ARVO abstract.

[65] R. Young. Pathophysiology of age-related macular degeneration. *Survey of Opthalmology*, 31(5):291–306, March-April 1987.